Title

A 2DRF pulse sequence for bolus tracking in hyperpolarized 13C imaging

Journal

Magnetic Resonance in Medicine, 74(2)

ISSN

0740-3194

Authors

Tang, Shuyu

Jiang, Wenwen

Chen, Hsin-Yu

et al.

Publication Date

2015-08-01

DOI

10.1002/mrm.25427

Peer reviewed

HHS Public Access

Author manuscript

Magn Reson Med. Author manuscript; available in PMC 2016 August 01.

Published in final edited form as:

Magn Reson Med. 2015 August ; 74(2): 506–512. doi:10.1002/mrm.25427.

A 2DRF Pulse Sequence for Bolus Tracking in Hyperpolarized ^{13}C Imaging

Shuyu Tang[1], **Wenwen Jiang**[1,2], **Hsin-Yu Chen**[1,2], **Robert Bok**[1], **Daniel B. Vigneron**[1,2], and **Peder E.Z. Larson**[1,2]

[1]Department of Radiology and Biomedical Imaging, University of California - San Francisco, San Francisco, California.

[2]UC Berkeley-UCSF Graduate Program in Bioengineering, University of California, San Francisco and University of California, Berkeley

Abstract

Purpose—A novel application of 2D spatially-selective radiofrequency (2DRF) excitation pulses in hyperpolarized ^{13}C imaging is proposed for monitoring the bolus injection with highly efficient sampling of the initially polarized substrate, thus leaving more polarization available for detection of the subsequently generated metabolic products.

Methods—A 2DRF pulse was designed with a spiral trajectory and conventional clinical gradient performance. To demonstrate the ability of our 2DRF bolus tracking pulse sequence, hyperpolarized [1-^{13}C]pyruvate in vivo imaging experiments were performed in normal rats, with a comparison to 1DRF excitation pulses.

Results—Our designed 2DRF pulse was able to rapidly and efficiently monitor the injected bolus dynamics in vivo, with an 8-fold enhanced time resolution in comparison with 1DRF in our experimental settings. When applied at the pyruvate frequency for bolus tracking, our 2DRF pulse demonstrated reduced saturation of the hyperpolarization for the substrate and metabolic products compared to a 1DRF pulse, while being immune to 0±5 ppm magnetic field inhomogeneity at 3T.

Conclusion—2DRF pulses in hyperpolarized ^{13}C imaging can be used to efficiently monitor the bolus injection with reduced hyperpolarization saturation compared to 1DRF pulses. The parameters of our design are based on clinical scanner limits, which allows for rapid translation to human studies.

Keywords

2DRF pulse; Reduced FOV imaging; ^{13}C; Hyperpolarized; MRI; Bolus tracking; Pyruvate

Introduction

Hyperpolarization refers to the redistribution of ordinary nuclei energy level populations to significantly enhance polarization (1). With hyperpolarization, the signal from a given

Address correspondence to: Peder Larson Byers Hall, Room 102C 1700 4th St San Francisco, CA 94158 TEL: (415) 514-4876 peder.larson@ucsf.edu.

number of nuclear spins can be raised by a factor of 10,000 or more when compared with equilibrium conditions at clinical field strengths (2). This dramatic increase in signal has the potential to substantially overcome the limited sensitivity of MR, thus allowing observing biomarkers with relatively low concentrations. Taking advantage of hyperpolarization and low natural abundance of ^{13}C, hyperpolarization of metabolically active compounds labeled with ^{13}C has been recently utilized for imaging metabolic processes in vivo with zero background signal (1, 3). The chemical shift of the ^{13}C nuclei can be used to distinguish between different molecular structures, producing separate images of the injected compound as well as its metabolic products. This has been used to observe increased conversion from [1-^{13}C]pyruvate to [1-^{13}C]lactate due to the Warburg effect in preclinical cancer models as well as in prostate cancer patients (4).

In hyperpolarized MR, the available magnetization must be utilized efficiently, as it is not replenished and experiences unrecoverable signal decay due to T1. It is also advantageous to observe the bolus delivery of the hyperpolarized substrate (e.g., pyruvate) to characterize the injection, perfusion, and for quantitative modeling. In this work, we proposed to use 2D spatially selective radiofrequency (2DRF) excitation pulses (5) to efficiently sample the initially polarized substrate, thus leaving more polarization available for detection as subsequently generated metabolic products. We believe this approach could be useful for monitoring the bolus injection and/or measuring an arterial input function for quantitative perfusion and kinetic modeling. It could be applied either on the vasculature or on tissue of interest and provide a measurement of physiologic differences in delivery and circulation between patients.

Previously, Vinding et al. (6) designed an optimal-control 2D RF pulse to improve the localization for hyperpolarized ^{13}C imaging. Our design is different from the Vinding et al work in terms of several key aspects. First, the motivation of our design is tracking a ^{13}C-labeled pyruvate bolus injection in vivo, therefore, our 2DRF pulse sequence was designed for a 3T clinical scanner with conventional gradient performances, which allows for rapid translation to human studies. In terms of acquisition methodology, Vinding et al. used a 180 degree refocusing slab pulse which could significantly reduce the hyperpolarized magnetization in the pulse or RF coil transition regions (7), and instead our approach used an echo-planar spectroscopic imaging (EPSI) readout (8) along the excited cylinder direction to localize to a specific voxel location. Similarly to Vinding et al, we utilized a spiral excitation trajectory, which leads to a blurred 2D profile for off-resonance metabolites. In vivo this is beneficial and leads to reduced hyperpolarization loss of metabolic products compared to conventional 1D RF pulses.

Methods

Our 2D spatially selective RF pulse was based on the k-space analysis (9) for small-tip angles (STA). Iterative (10), SLR (11), and optimal control (6) methods also could be used to design 2D RF pulses, which are particularly valuable for large-tip angles when the k-space method does not apply. Based on STA method, transverse magnetization can be expressed as a k-space integral, assuming the k-space trajectory does not cross itself.

$$M_{xy}(r,t) = iM_0 \int_k W(k)\, S(k)\, e^{-ikr} dk \quad [1]$$

where *W(k)* is a spatial weighting function,

$$W(k(\tau,t)) = (\gamma B_1(\tau)) / (|k(\tau,t)|) \quad [2]$$

and *S(k)* is a spatial frequency sampling function,

$$S(k) = \int_{-\infty}^{t} {}^3\delta(k(\tau,t) - k)\, |k'(\tau,t)\, d\tau \quad [3]$$

which determines the area and the density of the k-space representation.

Using Eq. 2, the required RF waveform can be calculated as

$$B_1(\tau) = W(k(\tau,t))\, |k'(\tau,t)\,| / \gamma = W(k(\tau,t))\, |G(\tau)\,| \quad [4]$$

We chose a constant-slew-rate inward spiral (Figure 1b) as the k-space trajectory (5) and a modulated Hamming-windowed jinc function (Figure 1d) as the weighting function, which generates an ellipsoid excitation profile. The gradient system was limited to 40 mT/m in gradient strength and 150 T/m/s in slew rate. RF and gradient waveform of our design are presented in Figure 1. Frequency offsets corresponding to 0.5 ppm inhomogeneity, [1-^{13}C]alanine and [1-^{13}C]lactate (relative to [1-^{13}C]pyruvate) at 3T were simulated in Matlab (Math-Works, Natick, MA) and tested on a spherical water phantom with our designed pulse built into a proton-imaging sequence. All 2D RF profile plots shown in the results are normalized by the maximum transverse magnetization of 5-degree flip. To examine the spatial selectivity of our design, our pulse was then built into a ^{13}C-MRSI sequence and validated on a ^{13}C phantom containing four different compounds in their own compartments: [1-^{13}C]alanine, [1-^{13}C]lactate, ^{13}C-formate, ^{13}C-bicarbonate (data not shown). Flow effects on the excitation in our design were simulated in a way similar to (12). To simplify the simulation, velocity profile in blood vessel hasn't been taken into consideration. Typical blood velocity values (13) in human vascular system are used in testing, since those values for rats are less available in literature.

To demonstrate the feasibility of our 2DRF bolus tracking pulse sequence, we tested it on the major vessels and kidneys of normal rats in hyperpolarized [1-^{13}C]pyruvate in vivo imaging experiments. They were performed on a GE 3T MR scanner with a custom, dual-tuned ^{13}C-^{1}H rat coil by injecting into a rat 2 mL of 100 mM [1-^{13}C]pyruvate pre-polarized in a HyperSense polarizer (Oxford Instruments). The sensitive, linear region of the coil was 4 inches long for ^{13}C and 5.75 inches long for ^{1}H coil, covering the entirety of the rat abdomen. All animal studies were carried out under a protocol approved by the UCSF Institutional Animal Care and Use Committee.

We compared a 2DRF-1DCSI (chemical shift imaging) versus 1DRF-2DCSI sequence with the same spatial resolution for imaging the bolus in the major vessels. This was to demonstraste the rapid acquisition feasible with 2DRF. Both RF pulses were targeted on the inferior vena cava (IVC) with 5-degree flip. 2DRF pulse (2.5 mm excitation resolution,

5mm excitation diameter, 10 cm excitation FOV) was normal to the axial plane while the 1DRF pulse was parallel to the sagittal plane. Chemical shift imaging (CSI) data was read out using an echo-planar spectral imaging (EPSI) sequence (8) localizing to $5 \times 5 \times 5$ mm^3 voxels. 1DCSI was along the superior-inferior direction while 2DCSI was applied on the coronal plane. We used a symmetric EPSI sequence, as described in (14), including ramp sampling, spectral resolution of 10.1 Hz, spectral bandwidth of 470 Hz and SNR efficiency of 94.5%. To achieve the same spatial resolution, the 1DRF-2DCSI required 8 phase encodes, which means it had a temporal resolution (2s) 8 times longer than 2DRF-1DCSI (250ms).

We also compared a 2DRF and 1DRF pulse in the kidneys. This was designed to demonstrate the feasibility of monitoring the bolus arrival to tissue, and also to assess the effects of the tracking pulses on the metabolite magnetization levels. Our 2DRF pulse (30-degree flip, 2.5 mm excitation resolution, 5mm excitation diameter, 10 cm excitation FOV) was targeted on the left kidney and normal to the coronal plane. The same EPSI readout sequence was performed for 24 s, which was followed by a $5 \times 5 \times 10$ mm^3 2D CSI in the axial plane at 30 s after bolus injection. This 2DCSI sequence was used to observe the effects of bolus tracking sequences on the metabolites' magnetization. A 1DRF pulse comparison study was performed with all other parameters kept the same. The right kidney signal was used for normalization to hyperpolarization and delivery, as it was not excited by either RF pulse. This also removes any effects of saturating blood pyruvates in the heart by the 1DRF.

Results

Figure 2 shows experimental results and simulation of excitation profiles produced using the designed 2DRF pulse and gradients waveforms. It can be noted that 0.5 ppm B0 inhomogeneity at 3T does not induce a dramatic change in the pattern and amplitude of the profile. Furthermore, we also found that T2* decay in the range of 10-50 ms did not noticeably change the shape of the pulse profiles (see Supplementary Material, Figure S1), but does reduce the peak excitation signal. For example, T2* = 30ms results in a 25 percent peak reduction. (We have typically measured in vivo linewidths of 10 Hz for hyperpolarized [1-^{13}C]pyruvate and [1-^{13}C]lactate at 3T, corresponding to T2* = 30 ms.) In contrast, frequency offsets corresponding to alanine and lactate at 3T significantly blur and reduce the peak excitation, which is attributed to the use of a spiral trajectory. The above results also indicate that when our designed RF is applied at the pyruvate frequency for bolus tracking, it will minimally perturb the metabolic products at off-resonance frequencies while being immune to 0±5 ppm magnetic field inhomogeneity at 3T. off-resonance effects on the ellipsoid excitation profiles are consistent with those of circular excitation profiles.

Figure 3 shows excitation profiles in the presence of in-plane flow. (Through-plane flow does not affect the profile.) At 40 cm/s, approximately the average velocity in the aorta and peak velocity in the inferior vena cava in humans, there is a noticeable shift and distortion of the excitation profile. At 80 cm/s (approximate peak aorta velocity), the shift is larger. Note that these cases would only be found if the 2DRF was placed perpendicular to the major

vessels. Our results show that velocities of 5 cm/s or lower would not cause dramatical profile shift (< 1mm) or excitation amplitude reduction.

To demonstrate the rapid acquisition of 2DRF, hyperpolarized [1-^{13}C]pyruvate experiments were performed with 1DRF and 2DRF "bolus tracking" pulse sequences applied on the major vessels. 1DRF-2DCSI uses phase encoding to localize to the same voxel size as the 2DRF-1DCSI acquisition. The latter one could achieve a much faster time resolution (250 ms) than the former (2s) because it did not require phase encoding. This allowed for observation of a rapid periodic oscillation of $\approx$1 Hz in the 2DRF pyruvate signal from the major vessels near the diaphragm (center voxel in Figure 4d) that we believe is due to the periodic respiratory motion causing the vessels to shift slightly relative to the 2DRF pulse location. The oscillations are much smaller and marginally observable in more inferior voxels away from the diaphragm (bottom voxel in Figure 4d). These voxels could be used for accurate bolus tracking. This rapid motion was not observed in the slower 1DRF-2DCSI acquisition.

Figure 5 shows the results of hyperpolarized ^{13}C experiments with 1DRF and 2DRF bolus tracking pulse sequence applied on kidneys, where a subsequent 2D CSI was acquired to assess the effects of the tracking pulses on the metabolite signal levels. A 30-degree flip angle was used for both pulses to accentuate any magnetization saturation. Similarly to major-vessels experiments, the ^{13}C-labeled pyruvate bolus arrival in the kidneys were clearly observed with both the 1DRF and 2DRF (Figure 4d). In the subsequent 2D CSIs, we observed a decrease in all three metabolite signal levels (20% in pyruvate, 28% in alanine and 16% in lactate) in the center of the left kidney when using the 1DRF compared to the more spatially selective 2DRF. This was normalized to the right kidney which accounts for polarization differences and also for any saturation of metabolites in the heart by the 1DRF pulses. We believe this larger consumption of the hyperpolarized magnetization with 1DRF was primarily due to a larger excitation region along the superior-inferior direction within the kidney. Another reason could be that the spiral excitation trajectory of the 2DRF minimally excited the off-resonance metabolites in the ROI. If the goal is to characterize the bolus in the smaller 2DRF excitation region, 1DRF causes unnecessary usage of hyperpolarization. Therefore, 2DRF is advantageous for bolus tracking and results in a greater SNR in subsequent imaging.

Discussion

Hyperpolarized ^{13}C experiments in major vessels and kidney demonstrate the ability of our designed 2DRF pulse sequence to perform fast and efficient bolus tracking. The use of 2DRF pulses helps improve localization which leads to reduced hyperpolarization saturation and enhanced time resolution. A spiral trajectory in excitation k-space makes our design selectively excite on-resonance metabolites while minimally saturating other off-resonance metabolic products and being robust to 0±5 ppm magnetic field inhomogeneity at 3T. We believe this approach could be useful for monitoring the bolus injection and/or measuring an arterial input function for quantitative perfusion and kinetic modeling. It could be applied either on the vasculature or on tissue of interest and provide a measurement of physiologic differences in delivery and circulation between patients.

In this application, the off-resonance profile blurring due to the spiral trajectory is advantageous for minimally perturbing other metabolites. Overall, this blurred profile still has the same total energy, but spread out over a larger region. When these 2DRF pulses are applied on the vessels, it is highly unlikely this blurred profile would coincide with anatomy to substantially saturate off-resonance metabolites. When applied on a tissue, this blurred profile will ensure that no metabolic products within the tissue of interest are perturbed.

Since a potential application of this technique is for bolus tracking, effects of spin motion on excitation and acquisition were investigated. In terms of excitation, as shown in the Figure 3, as long as magnitude of the in-plane velocity is smaller than 5 cm/s, there would be trivial dephasing effects. Through-plane motion along the 2D cylinder direction does not affect the pulse. So the most desirable location for bolus tracking is where bolus moves parallel to excitation cylinder. We also analyzed the EPSI acquisition, where the same velocities result in shifting of the signal and the decrease of spectral resolution proportional to the duration of the acquisition sequence (Figure S4). In this study, EPSI was used to confirm that off-resonance metabolites were not perturbed by 2DRF. Since we only observed a pyruvate peak, a spectroscopic imaging sequence was not necessary in 2DRF bolus tracking sequence. Thus, EPSI could be replaced with conventional spatial encoding sequence which would be much shorter and reduce the effects from spin motion, as shown in the middle column in Figure S4. In Figure 4, the signals might be distorted by spin motion. Since we were not able to monitor the flow velocity during the experiment, the flow effects cannot be directly evaluated. However, we observed strong alignment of spectral results to anatomy, indicating that the shifting effects caused by spin motion are small and our results are reliable. This could be explained by the right column of Figure S4 that shows a T2* decay of 30ms would reduce the signal shifting artifacts. Moreover, cardiac gating could be used to trigger the excitation when blood velocity is lowest. Gating could be especially useful for imaging the locations where blood flows in different directions (e.g. kidney) and the best orientation of excitation cylinder is hard to determine.

As with all spiral trajectories, this technique is sensitive to eddy currents and gradient delays. The excited ROI would appear rotated if the RF pulse and spiral do not match in time. From the results (Figure 2) of water phantom tests in our study, no rotation of excited ROI was observed. If necessary, gradient measurement techniques or delay calibration methods could be used to correct for gradient imperfections.

As presented in results, T2* decay will reduce the SNR for this method with in vivo hyperpolarized ^{13}C imaging. Figure S1 in the Supplementary Material provides a comparison among excitation profiles at different T2* values. It shows that shorter T2* results in more reduction in signal, because the RF energy is concentrated on the end part of RF pulse. Thus, to minimize T2* effects, the RF pulse duration should be as short as possible. A longer pulse duration will further blur the off-resonance profile but such a RF pulse will also be more susceptible to the main field inhomogeneity, as demonstrated in Figure S2. A larger FOV or ner excitation resolution would result in a longer pulse duration. A variable density spiral scheme introduced in the next paragraph could be used to achieve this.

In our 2DRF pulses, the excitation FOV (10 cm) is likely too small for human studies. A larger FOV would require a longer excitation pulse duration, which would be more susceptible to main field inhomogeneity as shown in Figure S2. However, a variable density spiral trajectory (15, 16) could be used to shorten the excitation duration without introducing substantial aliasing artifacts. Figure S3 shows that for a 20 cm excitation FOV, 2.5 mm excitation resolution pulse without variable density sampling, the ROI at 16 Hz B0 inhomogeneity has an amplitude less than half of the on-resonance profile, which would reduce SNR by the same amount. With quadratic variable density sampling, the pulse duration is similar to a 10 cm excitation FOV. But the inhomogeneity profiles do not have a significant improvement. This is because the pulse duration, 32ms, is longer than our estimated T2* of 30ms. For a 10 cm excitation FOV, our variable density sampling could shorten the pulse duration by three-fold to 10.3ms, now a third of this T2*. We can see that peak value in excitation profiles at an inhomogeneity frequency is at 75% of maximum possible peak, while excitation profiles corresponding to alanine and lactate at 3T significantly blur and have amplitudes less than 20% of maximum possible peak. This is good enough for selective imaging, considering the concentration of alanine and lactate is typically an order of magnitude smaller than pyruvate in hyperpolarized ^{13}C-labeled pyruvate experiments. Small aliasing ripples caused by undersampling in excitation k-space can be observed in the excitation profiles, which, in view of their small amplitudes (less than 10% of the on-resonance profile peak), we believe will not substantially contribute to the signal in hyperpolarized bolus tracking experiments. As an alternative to the variable density algorithm, parallel transmit techniques (17) could also be used to shorten RF pulse duration and acquire a large excitation FOV.

Recently there have been several reports on applying hyperpolarized ^{13}C for quantitative perfusion assessment (18, 19) as well as numerous applications of kinetic modeling. For quantitative perfusion imaging (19), a 2DRF can be placed on arteries and used for rapid measurements of the arterial input function. This would provide enhanced temporal resolution and reduced excitation saturation, while being more specific to the artery signal. For example, in Johansson's work (18), higher time resolution could give more accurate measurement of depolarization rate which is essential for better estimation of cerebral blood flow. Kazan et al have recently presented a highly accurate kinetic model using an arterial input function measured in continuous blood drawn from the femoral artery (20). A 2DRF could be directly targeted on the femoral artery to replace this invasive setup for measuring the arterial input function while minimally perturbing the magnetization for use in kinetic modeling.

Conclusion

We have successfully designed a 2DRF pulse to improve localization in hyperpolarized ^{13}C imaging and applied it to track the hyperpolarized ^{13}C-labeled pyruvate bolus in vivo, while minimally perturbing the metabolic products of lactate and alanine. The parameters of our design are based on clinical scanner limits, which allows for rapid translation to human studies.

Supplementary Material

Refer to Web version on PubMed Central for supplementary material.

Acknowledgements

We acknowledge National Institutes of Health funding R00-EB012064 and P41-EB013598 for support.

References

1. Kurhanewicz J, Vigneron DB, Brindle K, Chekmenev EY, Comment A, Cunningham CH, Deberardinis RJ, Green GG, Leach MO, Rajan SS, Rizi RR, Ross BD, Warren WS, Malloy CR. Analysis of cancer metabolism by imaging hyperpolarized nuclei: prospects for translation to clinical research. Neoplasia. 2011; 13:81–97. [PubMed: 21403835]
2. ArdenkjærLarsen JH, Fridlund B, Gram A, Hansson G, Hansson L, Lerche MH, Servin R, Thaning M, Golman K. Increase in signal-to-noise ratio of ¿ 10,000 times in liquid-state nmr. Proc Natl Acad Sci U S A. 2003; 100:10158–63. [PubMed: 12930897]
3. Golman K, in 't Zandt R, Thaning M. Real-time metabolic imaging. Proc Natl Acad Sci U S A. 2006; 103:11270–5. [PubMed: 16837573]
4. Nelson SJ, Kurhanewicz J, Vigneron DB, Larson PEZ, Harzstark AL, Ferrone M, van Criekinge M, Chang JW, Bok R, Park I, Reed G, Carvajal L, Small EJ, Munster P, Weinberg VK, ArdenkjaerLarsen JH, Chen AP, Hurd RE, Odegardstuen LI, Robb FJ, Tropp J, Murray JA. Metabolic imaging of patients with prostate cancer using hyper-polarized [1-c]pyruvate. Sci Transl Med. 2013; 5:198ra108.
5. Bottomley PA, Hardy CJ. Two-dimensional spatially selective spin inversion and spin-echo refocusing with a single nuclear magnetic resonance pulse. Journal of Applied Physics. 1987; 62:4284–4290.
6. Vinding MS, Laustsen C, Maximov II, Søgaard LV, ArdenkjaerLarsen JH, Nielsen NC. Dynamic nuclear polarization and optimal control spatial-selective 13c mri and mrs. J Magn Reson. 2013; 227:57–61. [PubMed: 23298857]
7. Josan S, Yen YF, Hurd R, Pfefferbaum A, Spielman D, Mayer D. Application of double spin echo spiral chemical shift imaging to rapid metabolic mapping of hyperpolarized [1-c]-pyruvate. J Magn Reson. 2011; 209:332–6. [PubMed: 21316280]
8. Mansfield P. Spatial mapping of the chemical shift in nmr. Magn Reson Med. 1984; 1:370–86. [PubMed: 6571566]
9. Pauly J, Nishimura D, Macovski A. A k-space analysis of small-tip-angle excitation. J Magn Reson. 1989; 81:43–56.
10. Hardy CJ, Cline HE. Broadband nuclear magnetic resonance pulses with twodimensional spatial selectivity. Journal of Applied Physics. 1989; 66:1513–1516.
11. Pauly J, LeRoux P, Nishimura D, Macovski A. Parameter relations for the shinnarle roux selective excitation pulse design algorithm [nmr imaging]. IEEE Trans Med Imaging. 1991; 10:53–65. [PubMed: 18222800]
12. Nishimura DG, Irarrazabal P, Meyer CH. A velocity k-space analysis of ow effects in echo-planar and spiral imaging. Magn Reson Med. 1995; 33:549–56. [PubMed: 7776887]
13. WEXLER L, BERGEL DH, GABE IT, MAKIN GS, MILLS CJ. Velocity of blood flow in normal human venae cavae. Circulation Research. 1968; 23:349–359. [PubMed: 5676450]
14. Yen YF, Kohler SJ, Chen AP, Tropp J, Bok R, Wolber J, Albers MJ, Gram KA, Zierhut ML, Park I, Zhang V, Hu S, Nelson SJ, Vigneron DB, Kurhanewicz J, Dirven HAAM, Hurd RE. Imaging considerations for in vivo 13c metabolic mapping using hyperpolarized 13c-pyruvate. Magn Reson Med. 2009; 62:1–10. [PubMed: 19319902]
15. Tsai CM, Nishimura DG. Reduced aliasing artifacts using variable-density k-space sampling trajectories. Magn Reson Med. 2000; 43:452–8. [PubMed: 10725889]

16. Lee JH, Hargreaves BA, Hu BS, Nishimura DG. Fast 3d imaging using variable-density spiral trajectories with applications to limb perfusion. Magn Reson Med. 2003; 50:1276–85. [PubMed: 14648576]

17. Zhu Y. Parallel excitation with an array of transmit coils. Magn Reson Med. 2004; 51:775–84. [PubMed: 15065251]

18. Johansson E, M ansson S, Wirestam R, Svensson J, Petersson JS, Golman K, St ahlberg F. Cerebral perfusion assessment by bolus tracking using hyperpolarized 13c. Magn Reson Med. 2004; 51:464–72. [PubMed: 15004786]

19. von Morze C, Larson PEZ, Hu S, Yoshihara HAI, Bok RA, Goga A, Ardenkjaer-Larsen JH, Vigneron DB. Investigating tumor perfusion and metabolism using multiple hyperpolarized (13)c compounds: Hp001, pyruvate and urea. Magn Reson Imaging. 2012; 30:305–11. [PubMed: 22169407]

20. Kazan SM, Reynolds S, Kennerley A, Wholey E, Bluff JE, Berwick J, Cunningham VJ, Paley MN, Tozer GM. Kinetic modeling of hyperpolarized 13c pyruvate metabolism in tumors using a measured arterial input function. Magnetic Resonance in Medicine. 2013; 70:943–953. [PubMed: 23169010]

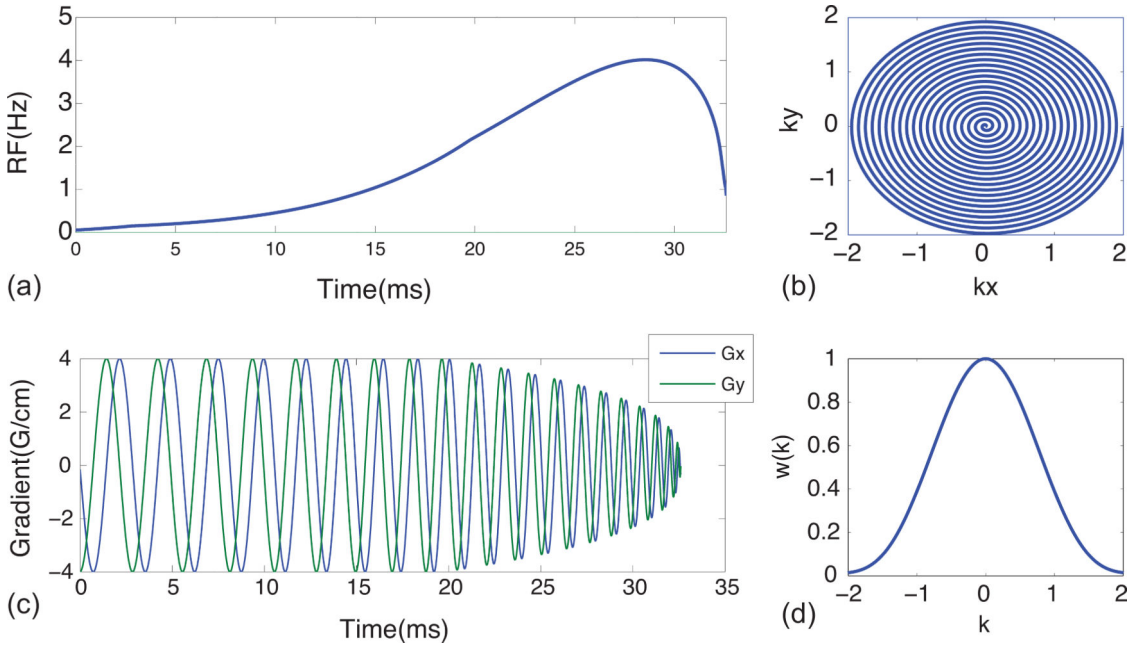

1.

(a) RF and (c) gradient waveform of our design, which generates a cylindrical profile with a 5-degree ip, 0.5 cm diameter, 0.25 cm resolution and 10 cm FOV. The gradient system was limited to 4 G/cm in gradient strength and 15 G/cm/ms in slew rate. The designed gradient waveforms and RF pulse were generated based on a spiral trajectory (20 turns) (b) and hamming-jinc weighting function in *k* space (d).

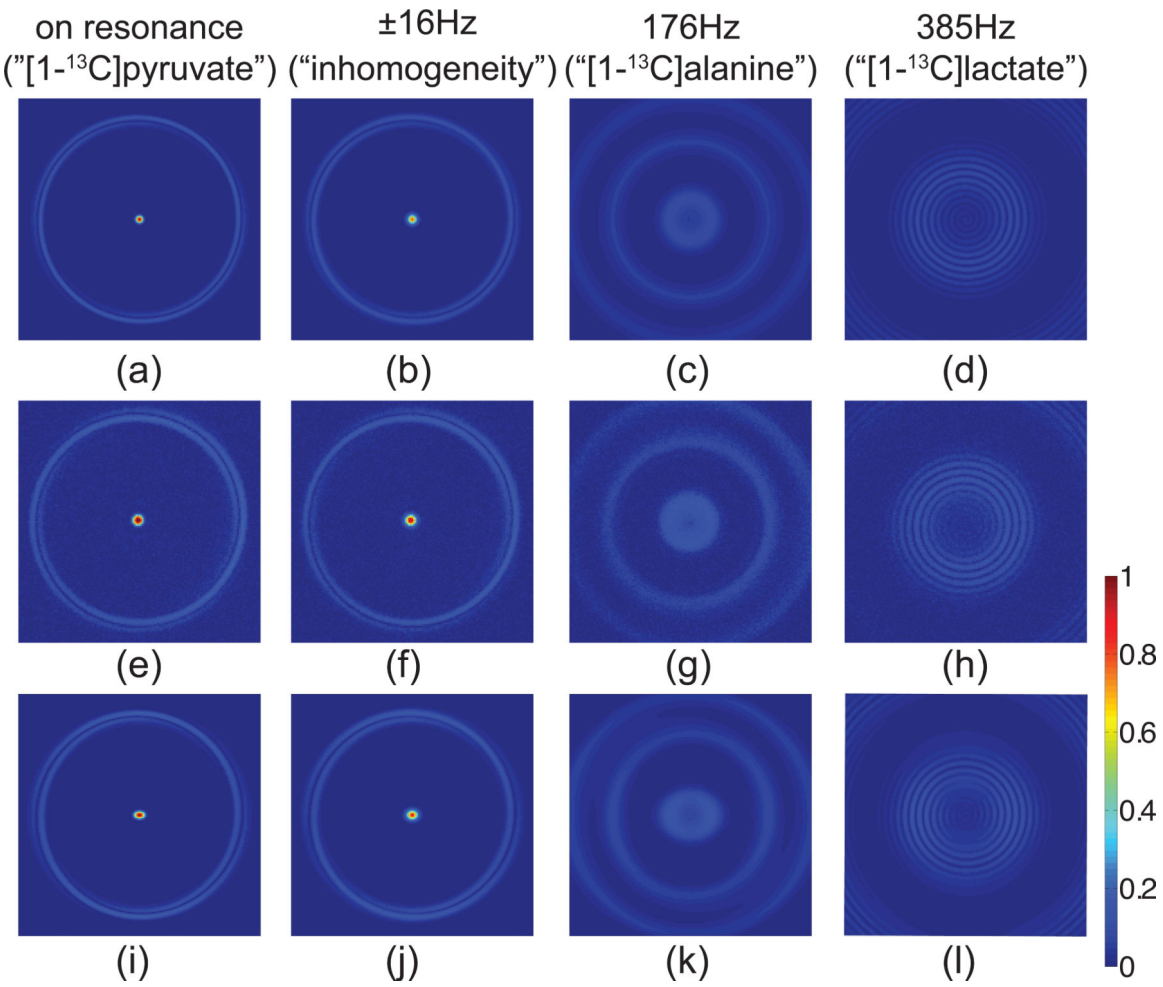

2.

Simulation and experimental demonstration of the designed 2DRF pulses, normalized by the peak on-resonance excitation. Graph (a-d) (dimension: 24 × 24 cm^2) are simulations of ^{13}C excitation profiles produced using the designed RF pulse and gradient waveforms in Figure 1 at on-resonance (a) and off-resonance (b-d) frequencies of main field inhomogeneity (±16Hz), [1-^{13}C]alanine (176Hz), and [1-^{13}C]lactate (385Hz) at 3T. Graph (e-h) (dimension: 6 × 6 cm^2) are results of ^{1}H imaging experiments on a spherical water phantom with all parameters except gymagnetic ratio the same as simulations in graph (a-d). Due to the difference in gymagnetic ratio, FOV in experimental results is four times smaller that in simulations. Graph (i-l) are simulations (dimension: 24 × 24 cm^2) of an ellipsoid selective volume (1 cm in horizontal axis and 0.5 cm in vertical axis) with all other parameters the same as in graph (a-d).

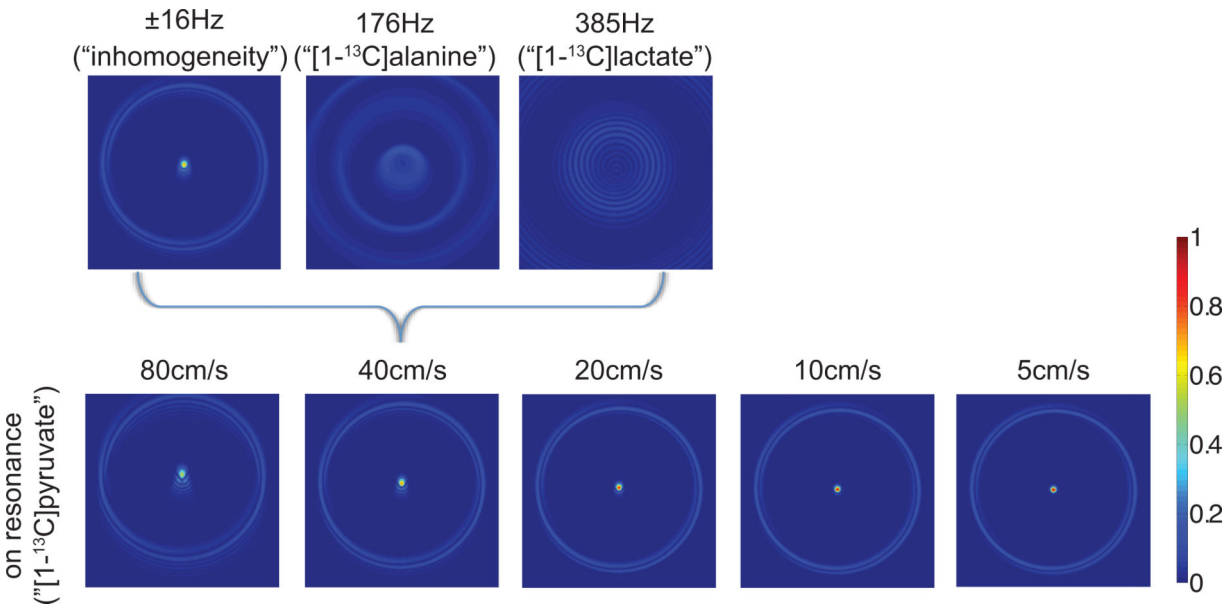

3.

Surface plots of excitation profiles of 2DRF pulse with tracked bolus at different in-plane velocities. All graphs have a dimension of 24 × 24 cm^2. The upper graphs are the simulated excitation profiles produced using the designed RF pulse and gradient waveforms in Figure 1 with tracked bolus at a in-plane velocity of 40 cm/s . The bottom graphs are on-resonance excitation profiles at velocities of 5 cm/s, 10 cm/s, 20 cm/s, 40 cm/s and 80 cm/s respectively, while keeping pulse shape and other parameters unchanged. As the speed increases, excitation profiles have more shift, less amplitude and more ringing effects.

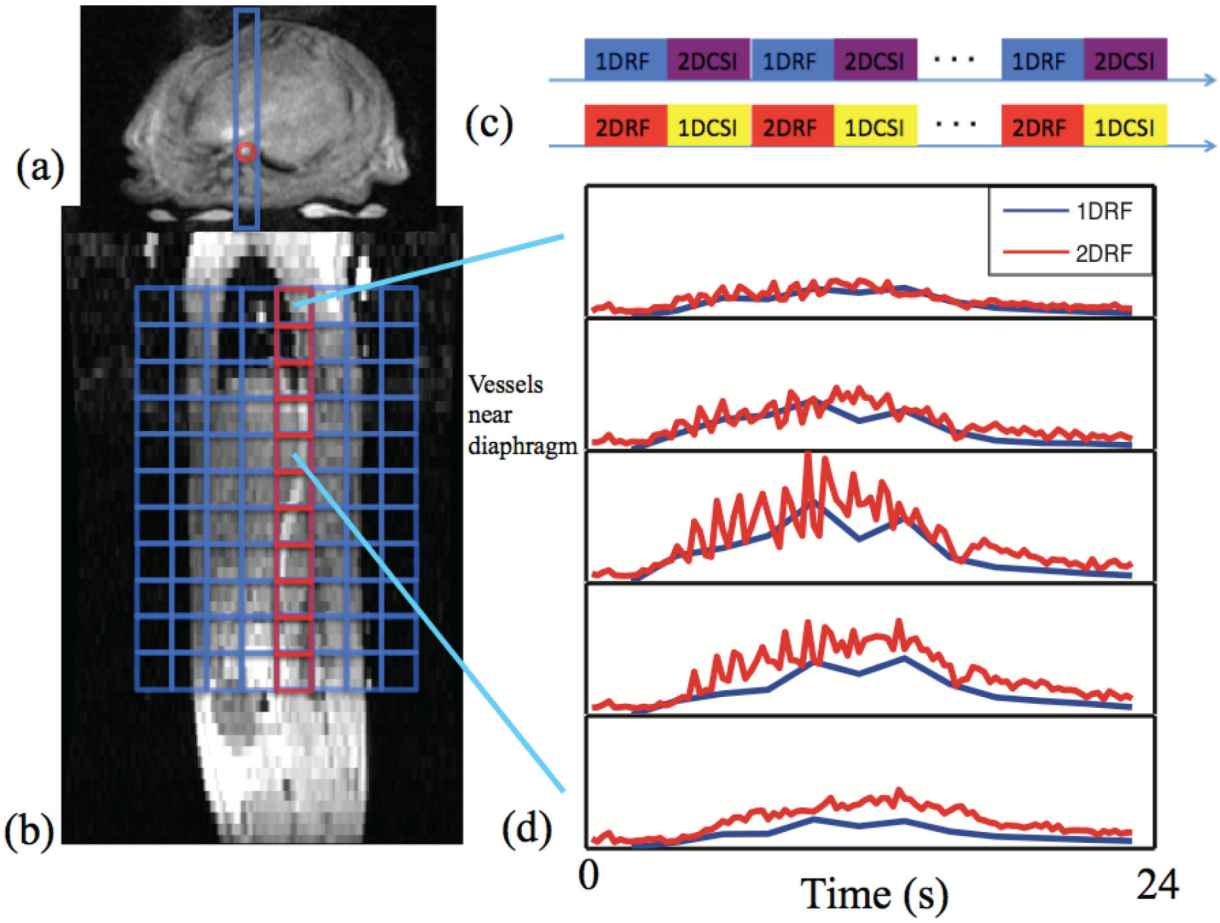

4.

Comparison of 1DRF and 2DRF ”Bolus tracking” sequence applied on the major vessels with the same spatial resolution in hyperpolarized 13C experiments. Due to phase encoding, the time resolution for the 1DRF-2DCSI was 2s, while the 2DRF-1DCSI was acquired every 250ms. This gure shows Bolus tracking sequence schematic diagram (c), excitation (a), acquisition scheme(b) and hyperpolarized 13C-labeled pyruvate signals (d) from voxels of targeted abdominal aorta. Oscillations with a 1 second period were observed in the pyruvate signal with 2DRF, which probably results from rat respiration.The voxels further away from the diaphragm do not show these oscillations and could be used for bolus tracking.

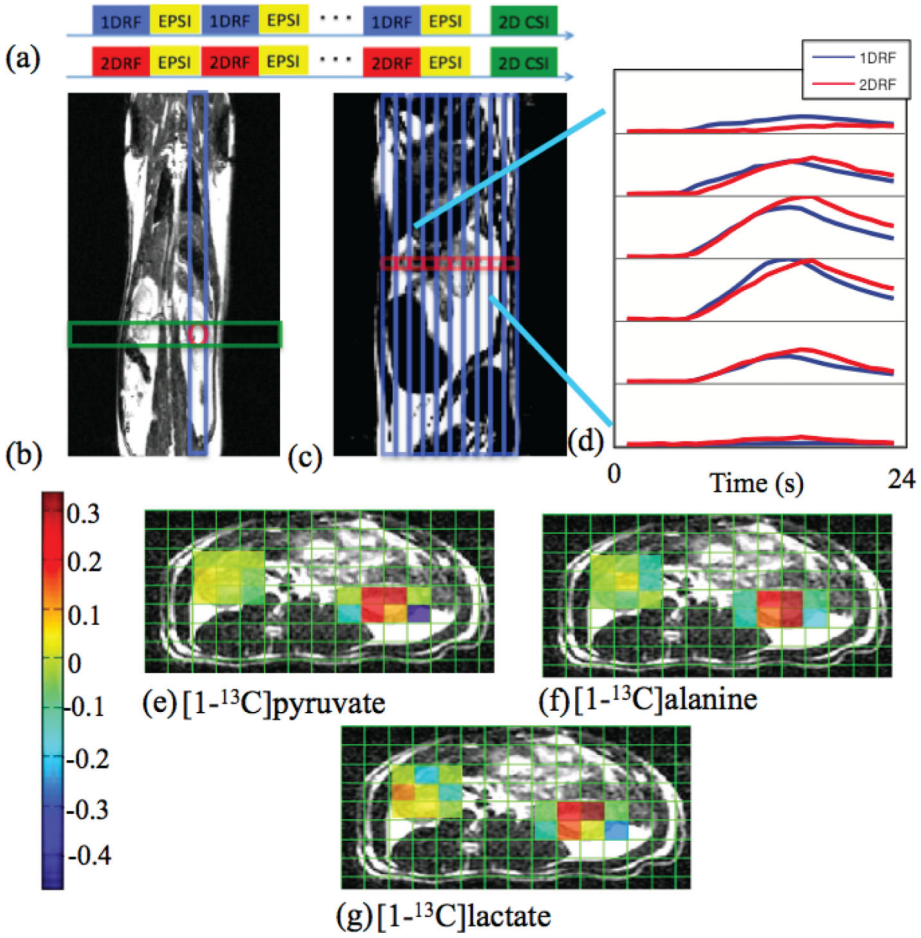

5.

Comparison of 1DRF and 2DRF ”Bolus tracking” pulse sequences and subsequent 2D CSI acquisitions applied on the left kidney with hyperpolarized 13C-pyruvate. The bolus tracking sequence (a) included 1D or 2D RF bolus tracking pulses (30-degree ip, TR = 1s) followed by a high-resolution 2D CSI acquisition to determine the effect of the tracking pulses on the metabolites magnetization. (b) Locations of the 1DRF (blue), 2DRF (red) and 2D CSI (green). (c) EPSI acquisition scheme. Hyperpolarized 13C pyruvate bolus injection signal (d) and 2D CSI comparison results (e-g). The maps are the percentage differences, (S(2D)-S(1D))/S(2D), between the CSI acquired after 2DRF (S(2D)) and 1DRF (S(1D) bolus tracking pulse sequences (normalized by the maximum signal in the right kidney). The mean value of the central four voxels that corresponds to the renal pelvis in the left kidney are 20%, 28%, and 16% for pyruvate, alanine and lactate metabolites signals, respectively, showing less saturation of all metabolites by the 2DRF in the left kidney due to its increased spatial selectivity.